Label-free evaluation of maturation and hepatotoxicity of human iPSC-derived hepatocytes using hyperspectral Raman imaging

Menglu Li[1,2†*], Yukiko Ueyama-Toba[3,4,5†], Matthew Lindley[1], Gunganist Kongklad[1,2,6], Yasunori Nawa[1,2], Yasuaki Kumamoto[1,4], Seiichi Ishida[2,7], Yasunari Kanda[2,8], Satoshi Fujita[1,2], Hiroyuki Mizuguchi[3,4,5], Katsumasa Fujita[1,2,4*]

AFFILIATIONS:

[1] Laboratory of Nanophotonics, Department of Applied Physics, Osaka University, 2-1 Yamadaoka, Suita, Osaka 565-0871, Japan.

[2] AIST-Osaka University Advanced Photonics and Biosensing Open Innovation Laboratory, National Institute of Advanced Industrial Science and Technology (AIST), 2-1 Yamadaoka, Suita, Osaka 565-0871, Japan.

[3] Laboratory of Biochemistry and Molecular Biology, Graduate School of Pharmaceutical Sciences, Osaka University, 2-1 Yamadaoka, Suita, Osaka 565-0871, Japan.

[4] Institute for Open and Transdisciplinary Research Initiatives, Osaka University, 2-1 Yamadaoka, Suita, Osaka 565-0871, Japan.

[5] Laboratory of Functional Organoid for Drug Discovery, Center for Drug Discovery Resources Research, National Institutes of Biomedical Innovation, Health and Nutrition, 7-6-8 Saito-Asagi, Ibaraki, Osaka 567-0085, Japan

[6] Department of Physics, Faculty of Science, Mahidol University, Bangkok 10400, Thailand

[7] Division of Applied Life Science, Graduate School of Engineering, Sojo University, 4-22-1, Ikeda, Nishi-ku, Kumamoto 860-0082, Japan.

[8] Division of Pharmacology, National Institute of Health Sciences, Kawasaki, Kanagawa 210-9501, Japan.

*Correspondence to: Menglu Li, Katsumasa Fujita

† Equal contributions

EMAIL: menglu.li@ap.eng.osaka-u.ac.jp; fujita@ap.eng.osaka-u.ac.jp

ABSTRACT

To promote the clinical application of human induced pluripotent stem cell (hiPSC)-derived hepatocytes, a method capable of monitoring regenerative processes and assessing differentiation efficiency without harming or modifying these cells is important. Raman microscopy provides a powerful tool for this, as it enables label-free identification of intracellular biomolecules in live samples. Here, we used label-free Raman microscopy to assess hiPSC differentiation into hepatocyte lineage based on intracellular chemical content. We contrasted this data with similar phenotypes from the HepaRG and from commercially available hiPSC-derived hepatocytes (iCell hepatocytes). We detected hepatic cytochromes, lipids, and glycogen in hiPSC-derived hepatocyte-like cells (HLCs) but not biliary-like cells (BLCs), indicating intrinsic differences in biomolecular content between these phenotypes. The data show significant glycogen and lipid accumulation as early as the definitive endoderm transition. Additionally, we explored the use of Raman imaging as a hepatoxicity and drug toxicity assay for the HepaRG and iCell hepatocytes, with data displaying a dose-dependent reduction of glycogen accumulation in response to acetaminophen. These findings show the non-destructive and high-content nature of Raman imaging provides a promising tool for both quality control of hiPSC-derived hepatocytes and hepatotoxicity screening.

INTRODUCTION

Liver diseases lead to approximately two million deaths per year, accounting for 3.5% of all death worldwide.[1] Hepatocyte and liver transplantation are the most effective treatments of liver diseases; however, donor shortage remains a worldwide problem. Less than 10% of patients can successfully find suitable transplants every year. Therefore, hepatocyte-like cells (HLCs) differentiated from stem cells[2,3,4] have received much attention as a potential source for hepatocyte transplantation, especially human induced pluripotent stem cells (hiPSCs),[5,6] due to their programmability, regenerative potential, and reduced ethical consideration.[7,8] The therapeutic efficacy of hiPSC-derived HLCs has been assessed in mice with liver injury, with improvements in cell viability and efficacy demonstrated for transplanted cell sheets rather than dissociated cell suspensions.[9] Also, the survival rate of mice with liver injury was increased by transplanting hiPSC-derived liver organoids.[10] The first clinical trial in human has been conducted using human embryonic stem cells (hESCs) derived hepatocytes to treat urea cycle disorder.[11] These demonstrations show stem cell differentiated hepatocytes have great potential for the treatment of liver diseases.

To promote the clinical application of HLCs from bench to bedside, a method capable of monitoring the regenerative processes and assessing cell populations without harming or modifying the cells is critical. Conventional methods using qRT-PCR, immunofluorescence staining, and western blotting can efficiently evaluate differentiation based on marker genes or proteins. However, since these methods generally require destructive treatment or the introduction of external labels, evaluated cells cannot be subsequently used for transplantation. A non-destructive and label-free method to monitor and evaluate live hepatocyte differentiation is necessary. In this regard, Raman microscopy has become a powerful tool for observing and discriminating cell type and tissue engineering in a label-free manner based on the chemically specific vibrations of intrinsic intracellular biomolecules.[12,13,14] For example, Hsu et al.

identified developmental stages of hiPSC-derived neurons by single-cell Raman-based spectroscopy combined with PCA analysis.[15] Brauchle et al. reported the non-invasive identification of cardiomyocytes from ESCs using Raman spectroscopy.[16] Several studies on stem cell-derived hepatocytes, including mesenchymal stem cells, ESCs, and iPSCs have also been investigated by Raman spectroscopy.[17,18,19] However, most studies analyzed cells or spheroids as a bulk sample using only spectral data not sensitive to the intracellular spatial distribution of biomolecules. Additionally, cytochrome information was limited in these studies due to the use of chemical fixation, which often oxidizes cytochrome, or the use of longer wavelength excitation (632.8 nm or 785 nm), which does not take advantage of cytochromes' strong resonance-Raman signal. We particularly note that cytochrome P450 (CYP), which constitute major drug metabolizing enzymes in hepatocytes, are expressed in HLCs but have not been previously detected in these cells with Raman measurement.

Traditionally, Raman measurement of cells and tissues suffers low sample throughput due to the inherently weak Raman cross section necessitating long acquisition times to produce a meaningful signal. The low throughput of Raman measurement is compounded in the imaging regime, which typically acquires a spectrum at each image-pixel by raster-scanning a laser focus across the image. This problem has been conquered with line-illumination Raman microscopy, which scans a line-shaped laser focus across the sample instead of a point-focus. The line-illumination regime acquires Raman spectra from several hundred image pixels at once, leading to a commensurate improvement to imaging speed over the point-focus method, making Raman imaging of large cell numbers and intracellular time dynamics possible. Line-illumination Raman has been used to study the dynamics of cytochrome *c* (cyt *c*) in cell mitosis and cell apoptosis, where cells were visualized without any additional sample preparations under 532 nm excitation.[20, 21] The technique has also characterized osteoblast differentiation based on real-time mapping of Raman signals from the osteoblastic mineralization product

hydroxyapatite,[22] and discriminated undifferentiated ECSs from differentiated cells.[23] In our previous study, we utilized line-illumination Raman imaging to evaluate hepatocyte quality by the non-destructive and label-free measurement of functional biomolecules, including cyt b_5, CYPs, glycogen, and lipids in differentiated HepaRG cells and primary human hepatocytes.[24]

In this study, we extend Raman imaging analysis to the longitudinal characterization of hepatic differentiation from hiPSCs across a typical 25-day stepwise process.[2, 25, 26] Without any destructive pretreatment, we performed label-free and live-cell Raman observation at each stage of hepatic differentiation. Functional molecules of hepatocytes were found to accumulate gradually as the hepatocytes differentiated and matured. Hyperspectral Raman imaging allowed the visualization of different developmental stages of hepatic differentiation, which correlated with conventional immunofluorescence staining and gene analysis methods, demonstrating the potential of label-free Raman microscopy for non-destructive assessment of hiPSC-derived hepatocytes. Additionally, we found Raman imaging also capable of high-content, quantitative analysis of drug hepatoxicity in hiPSC-derived hepatocytes, suggesting further applications for Raman imaging in hepatoxicity screening.

RESULTS

Hepatocyte-like cells (HLCs) generated from hiPSCs.

To differentiate cell samples from hiPSCs into hepatocytes, we followed a general stepwise differentiation mimicking the development process of the liver from endoderm differentiation, through hepatic specification, to hepatocyte differentiation and maturation. These steps were induced sequentially by adding different growth factors at each step, including activin A, morphogenetic protein 4 (BMP4)/ fibroblast growth factor 4 (FGF4), hepatocyte growth factor (HGF), oncostatin M (OsM), respectively (Figure 1a).

We first confirmed hepatic differentiation from hiPSCs on a quartz dish, as quartz is a suitable substrate for Raman observation. The undifferentiated state of hiPSCs was confirmed by NANOG staining (Figure 1b). After treatment with actinin A for 4 days, definitive endoderm (DE) cells were induced and differentiation efficiency was evaluated by staining of CXCR4, an endoderm cell marker. The hepatic specification was realized by replacing medium containing BMP4 and FGF4, which have essential roles in liver development. After treatment with BMP4 and FGF4 for 5 days, DE cells were differentiated into hepatoblast-like (HB) cells as determined by the detection of hepatocyte nuclear factor 4 alpha (HNF4α), a hepatocyte lineage marker. Further hepatocyte differentiation was performed by culturing in medium containing hepatocyte growth factor (HGF) for 5 days and following 11 days with OsM supplemented in the culture medium to further promote hepatocyte maturation. Mature hepatocyte markers, including albumin and CYP3A4, were expressed in HLCs colony. Gene analysis of *SOX2*, *SOX17*, *HNF4α*, *CYP3A4*, and *ALB* was performed at the different stages of hepatic differentiation and is shown in Figure 1c. A comparison of the profiles of gene expression for cells cultured on quartz versus conventional plastic plates is shown in Figure S1. A similar tendency was detected comparing hepatic differentiation on quartz dishes and plastic plates, indicating the successful differentiation of HLCs on quartz dishes.

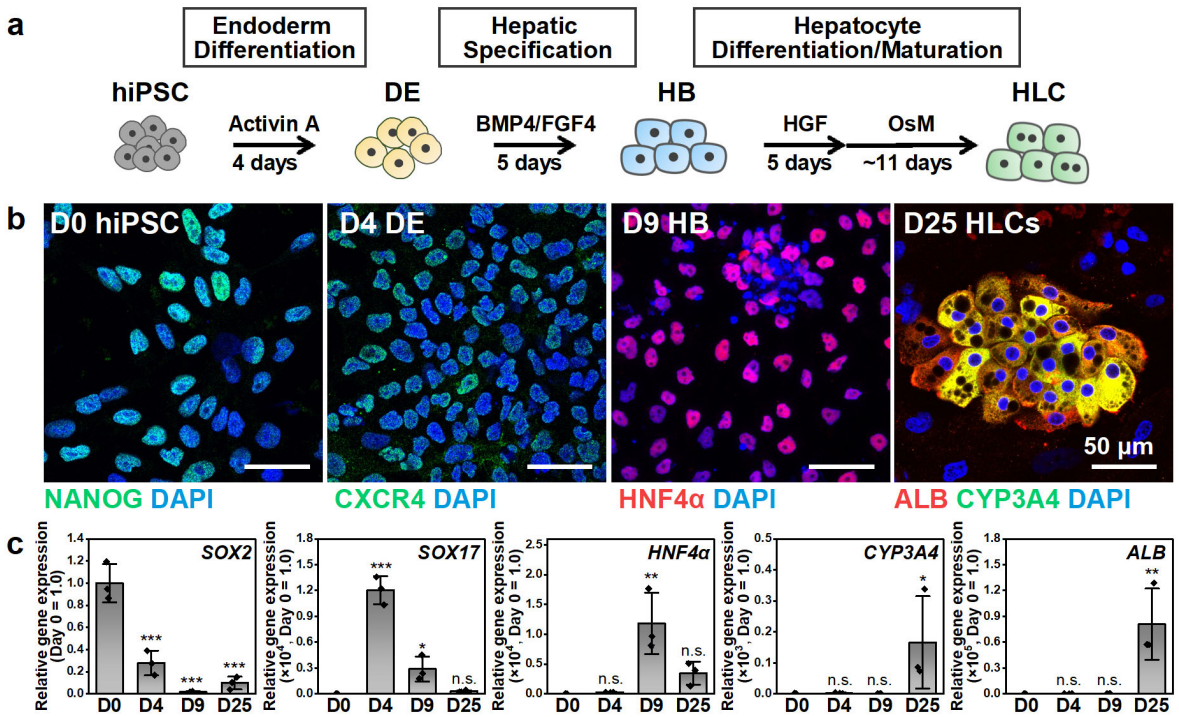

Figure 1 Generation of hiPSC-differentiated HLCs on quartz dishes. a A stepwise approach to generate HLCs through endoderm differentiation, hepatic specification, hepatocyte differentiation and maturation. **b** Immunostaining of cell markers of hiPSCs, definitive endoderm (DE) cells, hepatoblast-like (HB) cells, and HLCs, including NANOG, CXCR4, HNF4α, CYP3A4, and Albumin (ALB), respectively. Scale bars, 50 μm. **c** The gene expression levels of *SOX2*, *SOX17*, *HNF4α*, *CYP3A4*, and *ALB*. Results are shown as the mean ± SD (n = 3). Triplicate data points are shown as black diamonds in each bar. Statistical significance was evaluated by one-way ANOVA followed by post hoc Tukey–Kramer's range tests (compared with the left bar). n.s.: $P \geq 0.05$; *: $P < 0.05$; **: $P < 0.01$; ***: $P < 0.001$.

Raman profiles of hiPSC-derived HLCs

We used line-illumination Raman microscopy to characterize HLCs populations based on their intrinsic Raman profiles. The live HLCs were illuminated by a line-shaped laser light at 532 nm to record Raman spectra. Differentiated HepaRG cells with and without CYP induction were used as hepatocyte controls. A comparison of HLCs and HepaRG cells is shown in Figure 2. Since HLCs gave a strong lipid droplets signal, we separately compared the average spectra in the cytoplasm and lipid droplets. We used the fingerprint region (600~1800 cm^{-1}) for cytoplasm analysis (Figure 2a) and the CH-stretch region for lipid droplet analysis (Figure 2b). HepaRG cells, a model hepatocyte cell line which express high CYP amounts under induction were used as positive controls. HepaRG cells treated without inducer were used as a negative control. We looked for expected hepatic molecules, including cyt b_5 (675 cm^{-1}), glycogen (940 cm^{-1}), CYPs (1636 cm^{-1}) and lipid droplets (2850 cm^{-1}), which we identified in a previous study using HepaRG cells[24]. In addition, we simultaneously evaluated other molecules, like cyt *c* (642 cm^{-1}) that is related to mitochondrial activity but not specific to hepatocytes. Phenylalanine (1000 cm^{-1}), an essential amino acid, was visualized as a whole protein background.

Characteristic peaks that distinguish hepatocytes, including cyt b_5 and CYPs, were detected in HLCs. The intensity of CYP peak (1636 cm^{-1}) in HLCs is between the value of HepaRG with and without CYP induction. HepaRG cells can store glycogen and this ability is negatively related to the CYP induction[24]. In hiPSC-derived HLCs, we detected less glycogen compared to HepaRG cells (Figure 2c). The ability to accumulate fatty acids can be a marker of hepatocyte maturation and is well defined in hepatocytes.[27] We detected more and larger lipid droplets in HLCs than that in the HepaRG cells. Lipid droplets have been used as a maturation maker to identify HLCs differentiated from hESCs in stimulated Raman scattering

(SRS) microscopy.[18] Our data indicate a variance in CYPs, glycogen, and lipid accumulation between HLCs and HepaRG cells.

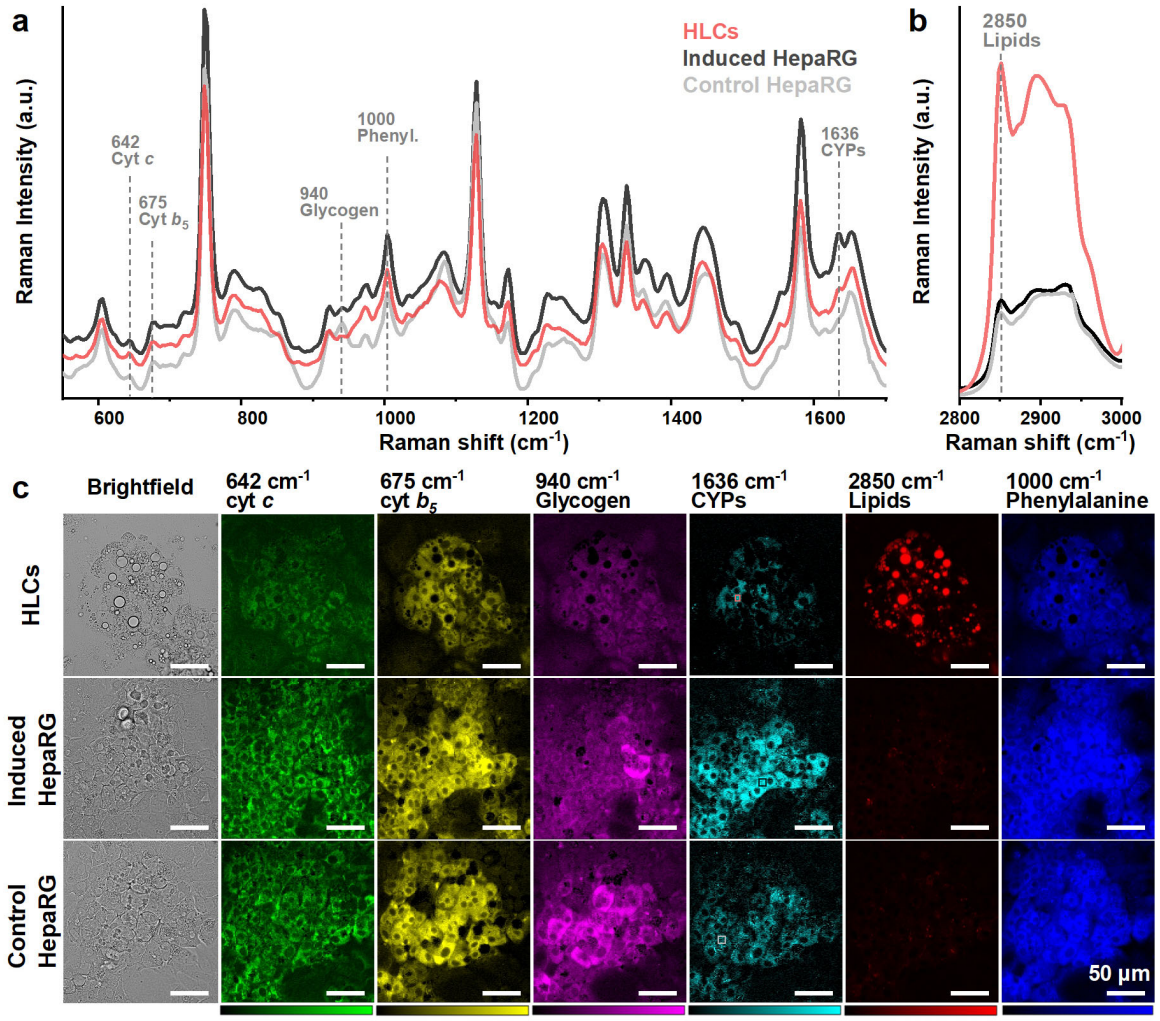

Figure 2 Raman profiles of HLCs and HepaRG cells. The average Raman spectra of HLCs, induced HepaRG cells and control HepaRG cells at cytoplasm (**a**) and lipid droplets area (**b**). The spectra are vertical shifted for comparison. The dotted lines at Raman shifts of 642, 675, 940, 1000, 1636, and 2850 cm^{-1} can be assigned to cyt *c*, cyt b_5, glycogen, phenylalanine, CYPs, and lipids, respectively. **c** The reconstructed Raman images at 642, 675, 940, 1000, 1636, and 2850 cm^{-1}. Averaged Raman spectra were extracted from the rectangle area indicated on Raman images at 1636 cm^{-1}. Scale bars, 50 µm.

Raman imaging of different cell populations in hepatic differentiation

After a 25-day differentiation, hiPSCs gradually differentiated into two cell populations in the same dish, including the CYP3A4-positive HLCs and CK-19 positive biliary-like cells (BLCs), as shown in Figure 3a. To investigate whether Raman microscopy can specifically identify these two cell populations, we collected Raman spectra from cytoplasm area of HLCs and BLCs regions, as indicated by red and gray squares. A clear difference in the averaged Raman spectra from these cell types can be distinguished, as shown in Figure 3b. The Raman spectrum of BLCs is dominated by the Raman scattering of cyt *c*, which can be identified by 642 cm^{-1} and 1314 cm^{-1}, with image contrast at these wavenumbers distinguishing mitochondria. These cyt *c* peaks were also present in the Raman spectrum of HLCs. We additionally identified the characteristic peaks of reduced b-type cytochromes, such as 675 cm^{-1} and 1304 cm^{-1}, which mainly comes from reduced cytochrome b_5 (cyt b_5) in hepatocytes. CYP expression is a marker of hepatocytes related to the major functions in clearing xenobiotics. We previously reported that the appearance of 1636 cm^{-1} corresponds to CYP induction and activity.[21] Here, we detected a 1636 cm^{-1} peak in HLCs but not BLCs (Figure 3c), which was consistent with the immunostaining of CYP3A4 (Figure 3d).

The reconstructed Raman images showing the localization of wavenumbers at 642 cm^{-1}, 675 cm^{-1}, 1636 cm^{-1}, and 2850 cm^{-1} demonstrate image-based characterization of the different cell types (Figure 3c). These images reveal heterogeneous cell populations in the final hepatocyte differentiation (at D25 hepatic differentiation), a detail which could not be distinguished in previous reports using bulk analysis via conventional Raman spectroscopy without spatial information. Moreover, the Raman-based method agreed with in situ immunofluorescence staining (Figure 3d), which has been widely used to identify the different cell types. Thus, we show that Raman imaging is capable of characterizing hiPSC-derived cell products without fixation and in a label-free manner.

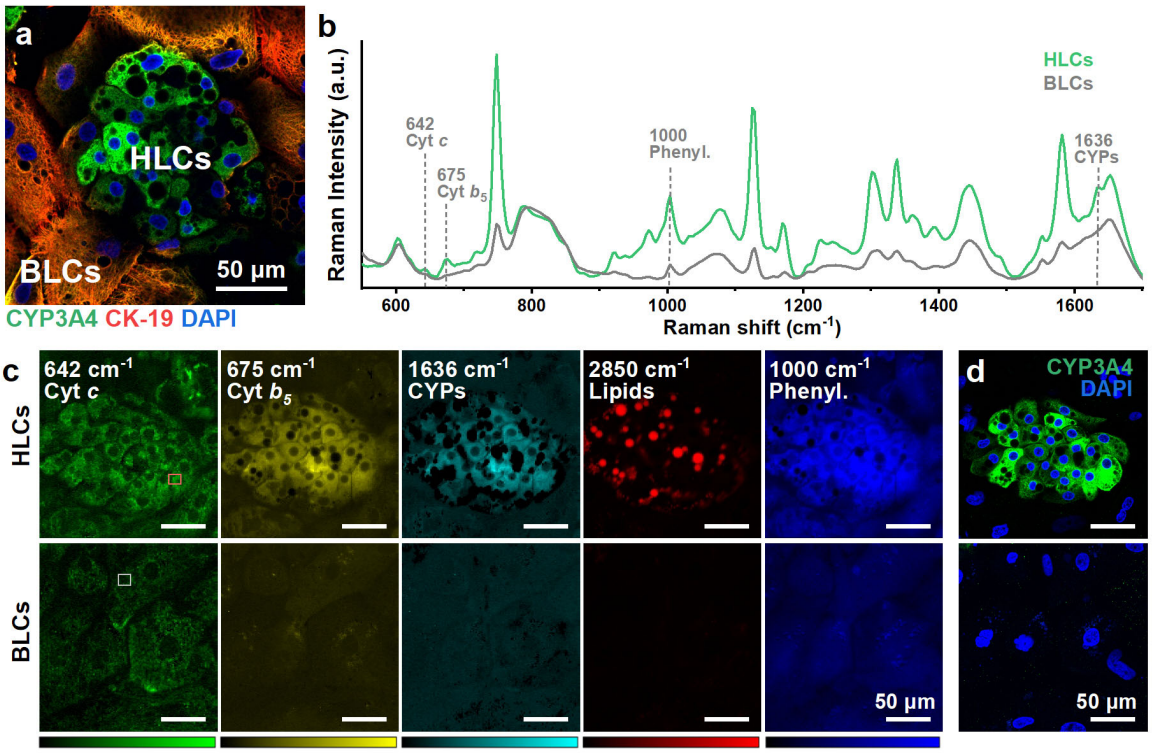

Figure 3 Comparison of HLCs and biliary-like cells (BLCs). a Immunofluorescence staining of CYP3A4 and CK-19 indicates the existence of HLCs and BLCs. **b** Average Raman spectrum of HLCs and BLCs. **c** Reconstructed Raman images at 642 cm^{-1}, 675 cm^{-1}, 1636 cm^{-1}, 2850 cm^{-1}, and 1000 cm^{-1} were indicated, which can be assigned to cyt *c*, cyt b_5, CYPs, lipids, and phenylalanine. **d** The immunofluorescent image of CYP3A4 obtained by a confocal fluorescence microscope at the same position as Raman observation. Scale bars, 50 μm.

Label-free evaluation of hepatic differentiation.

Next, we monitored the stepwise differentiation towards hepatic lineage using a line-illumination Raman microscope. Time-course Raman imaging was performed at D0, D4, D9, and D25 of the differentiation to obtain Raman spectra of hiPSC, DE, HB, and HLCs, respectively. To reduce the possible laser damage on differentiation, separate dishes at different stages were utilized in this study. Using the multiplex spectral detection capability of line-illumination Raman microscopy, we obtained enough spectra to study the changes quantitatively. Under our experimental conditions, we measured triplicate dishes with 3~4 Raman images per dish. Each Raman image contains 50400 Raman spectra at an acquisition time of 20 min. To compare among different cells, we extracted spectra from the cell area (and excluded non-cell area) for hiPSC, DE, HB. We note that, for HLCs, we extracted only cell areas with a 1636 cm^{-1} peak above the baseline to avoid immoderate contributions from the large lipid droplets. In total, Raman spectra of hiPSC, DE, HB, and HLCs were averaged from 235168, 424374, 347537, and 92658 spectra, respectively, shown in Figure 4a. The Raman spectrum of HLCs showed the most changes compared to other stages, especially in strong signals at 675, 750, and 1636 cm^{-1}, which can be respectively assigned to reduced cyt b_5, all cytochromes, and CYPs. These chemicals all relate to mature hepatic functions, and they were dominant among averaged spectra at the final stage of differentiation. A quantitative analysis of time-course spectra demonstrated the same tendency (Figure 4b).

Apart from the big change in HLCs, we also found significant spectral changes during differentiation from D0 hiPSC to D4 DE after only four days of activin A treatment. High-resolution Raman images of 642, 940, 2850 cm^{-1}, respectively assigned to cyt *c*, glycogen, and lipids, are shown in Figure 4c. hiPSCs showed strong cyt *c* (642 cm^{-1}) than DE cells, which may relate to their rapid division and self-renewal ability.[28] Glycogen (940 cm^{-1}) granules were found in hiPSCs, as reported previously.[29] After replacing to DE inducing medium for four

days, cyt *c* decreased and more glycogen was accumulated. An increasing in lipid droplets has been reported as a Raman indicator of ESCs cells undergoing differentiation.[23] In agreement with the previous report, we detected lipid droplets (2850 cm^{-1}) in DE cells but not in hiPSCs. The Raman spectra extracted from cytochrome-rich, glycogen-rich, and lipid-rich area are shown in Figure 4d, with the characteristic peaks assigned to these molecules indicated. The decrease in cyt *c* and increase in glycogen amounts at the initial step of hepatic differentiation were confirmed by conventional methods using immunofluorescence staining (Figure 4e) and Periodic acid-Schiff (PAS) staining (Figure 4f).

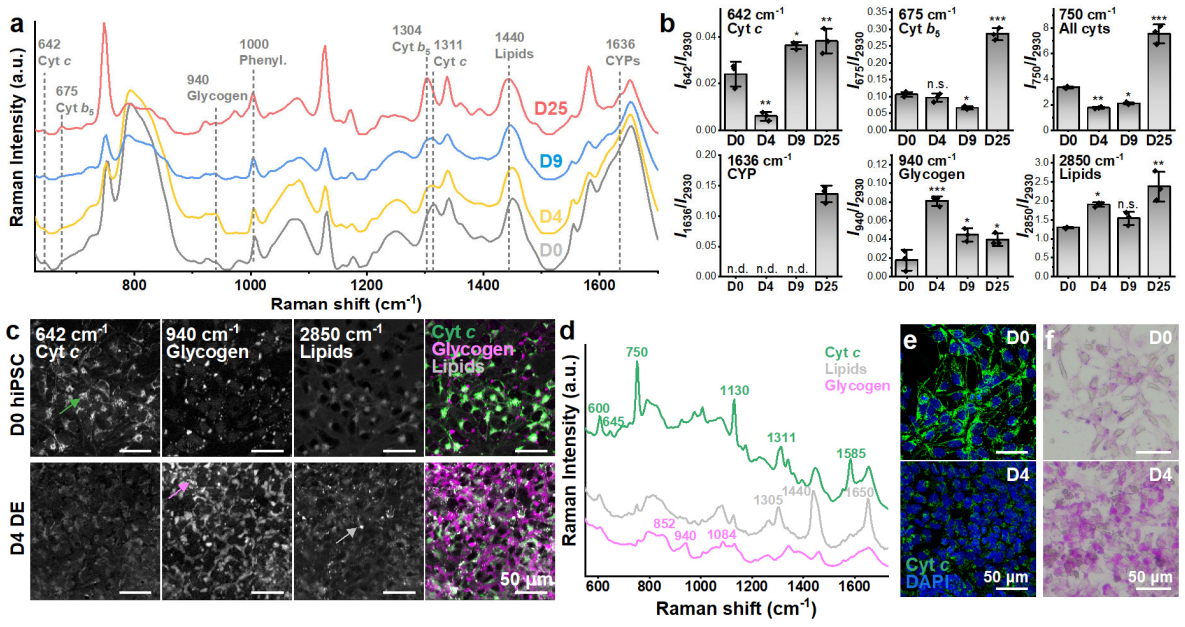

Figure 4 Time-course Raman profiles of hepatic differentiation and changes at early phase. a Transition of Raman spectra in the cell lineages: D0 hiPSCs (gray trace), D4 DE cells (yellow trace), D9 HB cells (blue trace), and D25 HLCs (red trace). The spectra were normalized to the peak area of 2930 cm^{-1}, assigned to CH_3 vibration, and generally used as cell reference band. **b** Quantification of Raman characteristic peaks at 642, 675, 750, 1636, 940, 2850 cm^{-1}, which can be assigned to cyt *c*, cyt b_5, all cyts, CYPs, glycogen, and lipids, respectively. 1636 cm^{-1} signal was not detected (n.d.) in D0, D4, and D9 of hepatic differentiation. Results are shown as the mean ± SD (n = 3). Triplicate data points are shown as black diamonds in each bar. Statistical significance was evaluated by one-way ANOVA followed by post hoc Tukey–Kramer's range tests (compared with the left bar). n.s.: $P \geq 0.05$;

*: $P < 0.05$; **: $P < 0.01$; ***: $P < 0.001$. **c** Reconstructed Raman images indicates early changes of DE differentiation at 642, 940, and 2850 cm^{-1}. **d** Raman spectrum of cyt-, glycogen-, and lipid-rich spots indicated by green, magenta, and gray arrows in **c**. **e** Immunofluorescence staining of cyt *c* indicates decrease of cyt *c* during the transition from hiPSC to DE. Cell nuclei were counter stained using DAPI. (**f**) PAS staining shows the clear accumulation of glycogen from hiPSC to DE. Scale bars, 50 μm.

Characterization of iCell hepatocytes

To investigate if Raman microscopy is applicable to other hiPSC-derived hepatocytes, iCell hepatocytes, a commercially available hiPSC-derived hepatocyte line with long-term CYP activity, glycogen storage, lipid metabolism, and potential to screen hepatotoxicity, were evaluated using Raman imaging. Under the culture condition suggested by the manufacturer, CYP expression gradually increases.[30] To characterize this process, we cultured iCell hepatocytes with the manufacturer-recommend protocol and performed time-course observation using Raman microscopy. We observed two dishes with 3~4 positions containing 120, 90, 117, and 80 cells at Day 3, Day 5, Day 7, and Day 9, respectively. We simultaneously visualized the increase of Raman signals at 1636 and 940 cm^{-1}, which can be assigned to CYPs and glycogen (Figure 5a). Raman observation was consistent with CYP3A4 activity assay (Figure 5b), CYP3A4 immunofluorescence staining (Figure 5c), and PAS staining (Figure 5d).

Lipid accumulation is a characteristic of mature hepatocytes. Conventionally, dyes including Oil red O and BODIPY, are used to detect lipid accumulation. Raman microscopy has been widely used as a label-free method for lipid measurement via the detection of CH_2 and CH_3 vibrations at Raman shifts of 1440 cm^{-1}, and 2850 cm^{-1}, which are abundant in long fatty acid chains.[31] We detected more lipid droplets in iCell hepatocytes treated with a mixture of free fatty acid (FFA, palmitic acid: oleic acid = 1:2) for 24 h (Figure 5e). A drastic increase of lipid droplets is shown in the Raman images at 2850 cm^{-1}. Quantitative analysis of lipid

peaks at 2850 cm^{-1}, assigned to CH_2 bending, showed a significant increase after treatment with fatty acid mixture, while 1000 cm^{-1}, which can be assigned to whole protein content, remained constant (Figure 5f).

iCell hepatocytes have been reported to respond to drug treatment in a manner similar to primary hepatocytes, but to be more resistant to hepatotoxic drugs such as acetaminophen (APAP). We detected no significant change in an ATP assay after treating iCell hepatocytes with APAP until 10 mM for 24 h (Figure 5g), which is consistent with previous literature.[32] We likewise performed quantitative analysis of Raman signals of 642, 675, 1636, 940, 1440 cm^{-1}, which can be assigned to cyt *c*, cyt b_5, CYPs, glycogen, and lipids, respectively. Similar to the result of ATP assay, peak intensities of 642, 675, 1636, 1440 cm^{-1}, were constant even until 10 mM APAP treatment (Figure 5h). No significant changes were found in cell morphology or Raman images of these wavenumbers (Figure S3). Interestingly, we found 940 cm^{-1} gradually decrease from 0 to 10 mM APAP treatment. This result shows APAP treatment did not alter ATP amount but did decrease glycogen accumulation significantly at 5 mM APAP. This finding agrees with the previous literature showing APAP treatment depleted hepatic glycogen and cause hyperglycemia.[33] We expanded this analysis to HepaRG cells and found a drastic decrease of ATP amount at 2.5 mM APAP. We found a decrease in cyt b_5, glycogen and CYPs among HepaRG cells compared to their iCell counterparts (Figure 5h). But a significant increase in reduced cyt *c* was detected at 10 mM APAP in HepaRG cells, which may relate to the reduction activity of APAP metabolite intermediates.[34]

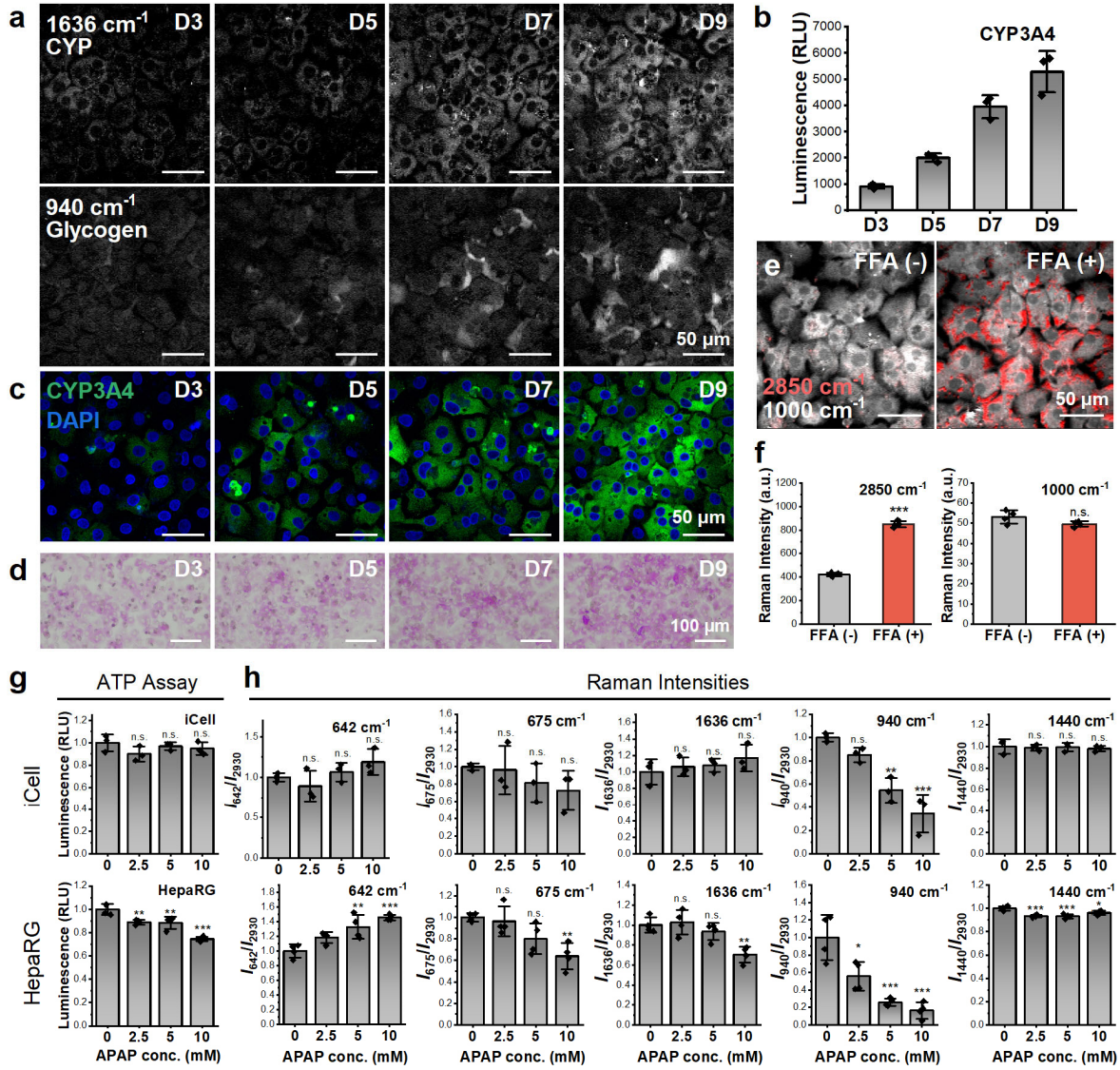

Figure 5 Raman characterization of iCell hepatocytes in hepatotoxicity assay. a Time-course Raman images of iCell hepatocytes captured at D3, D5, D7, and D9. Scale bars, 50 μm. **b** CYP3A4 activity assay indicates the increment of CYP3A4 activity during the culture. **c** Immunostaining of CYP3A4 with nuclei counterstained with DAPI. **d** PAS staining. **e** Merged Raman images of iCell hepatocytes treated with and without 500 μM free fatty acids (FFA, palmitic acid: oleic acid = 1:2), indicated using FFA (+) and FFA (-), respectively. Red color is for 2850 cm^{-1} (lipids) while gray scale is for 1000 cm^{-1} (protein). **f** Quantification of Raman peaks at 2850 and 1000 cm^{-1}, indicating a significant increase in lipid droplets after FFA treatment while whole protein amount remained constant. **g** Raman analysis indicates more drug resistance in iCell hepatocytes compared with HepaRG cells, which is consistent with an ATP assay. The values are normalized to the most left column. **h** High-content Raman

measurement of hepatic molecules after APAP treatment. The values are normalized to the most left column. Statistical significance was evaluated by one-way ANOVA followed by post hoc Tukey–Kramer's range tests (compared with the left bar). n.s.: $P \geq 0.05$; *: $P < 0.05$; **: $P < 0.01$; ***: $P < 0.001$

DISCUSSION

This research provided a Raman image-based evaluation of hepatic differentiation from hiPSCs and monitored the differentiation process. Compared to conventional spectroscopy-based monitoring, our line-illumination imaging modality visualized hepatic molecular content at a spatial resolution comparable to confocal fluorescence microscopy without external labels. Raman measurement of HLCs detected typical hepatocyte Raman spectra, however, we found the peak intensities of these spectra, corresponding to intracellular molecular content, varied compared to the peak intensities from the hepatocyte model cell line HepaRG. HLCs showed an overall lower glycogen and CYP expression but a higher lipid accumulation when compared with to the HepaRG cells (Figure 2). At the final differentiation state, HLCs and BLCs could be distinguished based on intracellular content, including cyt b_5, CYPs, and lipids (Figure 3). We found measurement of the Raman bands from these molecules can evaluate the efficiency of hepatic differentiation at a non-destructive and live-cell format.

Monitoring cell differentiation without any labels or invasive treatment is an important goal for the practical application of regenerative medicine. Our label-free imaging was sensitive to the resonance Raman signal from CYP, a major metabolizing enzyme in hiPSC-differentiated hepatocytes. We found that high-resolution Raman imaging distinguished the CYP-positive colony and CYP-negative surrounding cells based on molecular content, and we confirmed this with immunofluorescence staining (Figure 3). A time-course increase of CYP expression was detected in iCell hepatocytes that was consistent with CYP3A4 activity assays (Figure 5b) and immunofluorescence staining (Figure 5c). This suggests that Raman detection

of CYPs can provide a non-destructive maturation marker of hepatic differentiation comparable to conventional activity assay or immunofluorescence staining. The appearance of the CYP peak occurred at the final stage of differentiation (Figure 4b), which was consistent with gene analysis (Figure 1c). During the time course, we also detected hepatic lipid and glycogen accumulation which agreed with previous studies.[18,19] We found that cells which displayed lipid accumulation right after OsM treatment had an increased probability to become CYP-positive HLCs (Figure S2). This is related to the function on OsM in triggering lipid metabolism as well as CYP expression,[35,36] facilitating the differentiation and maturation of HLCs.

Previous Raman-based analysis of hiPSC-derived hepatocytes utilized spectroscopy of bulk biological samples and lacked spatial information, making it difficult to tease subtle molecular information from the averaged spectra.[17,18,19] When combining Raman spectroscopy with imaging, a clear spatial distribution of spectra between cell types and intracellular positions is made apparent. This facilitates the biological interpretation of acquired spectra by allowing in situ confirmation using conventional staining methods such as immunofluorescence staining (Figure 3d). Also, glycogen granule shape and location in both Raman images and PAS staining confirmed the existence of glycogen as a granule shape in hiPSCs (Figure 4c). While these granules have been reported previously for hiPSCs,[29] our data shows accumulation increases after differentiation to early definitive endoderm cells (Figure 4c and 4e).

The variation of glycogen amount has been previously associated with the different pluripotent states of hiPSCs[37] and the abundant glycogen in endoderm cells in the human yolk sac has been reported.[38] This suggests possible roles for glycogen in endodermal differentiation. Although definitive endoderm cells are defined by several markers, including SOX17, CXCR4, the glycogen storage has not been reported in literature focusing on definitive endoderm

differentiation. In our research, DE formation was induced by adding activin A, a Nodal signaling alternative protein, binding to the receptor of Nodal protein. Not only Nodal signaling, activin A was also reported to promote the gene expression of *WNT3*,[39] a gene for WNT3a protein, which is associated with the Wnt signaling pathway. The increase of WNT3a protein might activate the Wnt signaling and result in phosphorylation of glycogen synthase kinase 3 (GSK-3). GSK-3 inhibits glycogen synthase, and the phosphorylation of GSK-3 leads to the activation of glycogen synthase, inducing glycogen accumulation in cells. This signaling pathway may be associated with the accumulation of glycogen among DE cells found in our study, suggesting glycogen accumulation can be an endoderm marker. As far as we know, it is not yet used in this manner. Fraga et al. reported the increase of glycogen amount during early development of embryogenesis using the model organism Red Flour Beetle.[40] Although clarifying the detailed mechanism and function of glycogen accumulation in the endoderm differentiation is beyond the scope of this work, we found Raman microscopy can detect dynamic changes of glycogen in live cells, which is useful as a definitive endoderm marker to evaluate hepatic differentiation at the early differentiation stage.

Hepatotoxicity screening is a major topic in pharmaceutical research. Using hiPSC differentiated hepatocytes for hepatoxicity screening overcomes the intrinsic limitation of primary hepatocytes, which lose function once plated, reducing their ability to evaluate long-term toxicity and drug resistance. However, hepatotoxicity is a multicellular and multifactorial pathological process, and the simultaneous detection of various reporters for cell toxicity without interrupting cell homeostasis remains a challenge. Here we have shown that the label-free nature of hyperspectral Raman imaging provides a useful method for hepatotoxicity screening among hiPSC-derived hepatocytes. Our method allowed the effect of drug dose on various hepatic molecules to be evaluated simultaneously, and the data suggest glycogen depletion serves as an earlier and more sensitive toxicity marker than conventional ATP assay

(Figure 5g and 5h) when evaluating APAP toxicity. This is consistent with previous studies.[33,41] We believe this method can be extended to toxicology testing of other drugs that act on the biological pathways of our detected hepatic molecules, with measurement performed on live cells under physiological relevant conditions and without tedious staining processes.

Chemical imaging using Raman microscopy has shown a great potential in regenerative medicine, but high-resolution Raman imaging is traditionally limited by the low signal of Raman scattering, reducing typical sample throughput to one cell per several hours for point-focus-based microscopy. Using our line-illumination Raman microscope, hyperspectra from 400 image pixels were acquired during a single exposure of 5s, such that each Raman image is comprised of 50,400 spectra captured in less than 20 min. This allowed a sampling throughput high enough for statistical analysis, such as 3~4 positions in one dish and 3~4 dishes per condition. Hundreds of live cells per condition were observed, which would not be possible in a realistic time frame with the conventional point-focus method. This non-destructive and live-cell feature of Raman imaging make this technology well-suited in regenerative medicine and cell therapy. We believe our microscope pushes Raman imaging a step closer to screen live cells at high throughput and in a high-content manner for quality control in regenerative cell therapies.

In conclusion, hyperspectral Raman imaging clearly visualized intracellular molecular content during different developmental stages of hepatic differentiation, delineated these stages, and provided new insights into hepatoxicity testing. This demonstrates the potential of label-free Raman microscopy for non-destructive and high-content assessment of hiPSC-derived hepatocytes. In the future, this technique could be a valuable tool for the quality control of hiPSC-derived hepatocytes as well as for the assessment of hepatotoxicity.

METHODS

Maintenance culture of hiPSCs

The hiPSC line, YOW iPSCs[42] were maintained in on culture dishes pre-coated with iMatrix-511 (recombinant human laminin 511 E8 fragments, Nippi) at a density of 1 μg/cm2. The hiPSCs were maintained in StemFit AK02N medium (Ajinomoto) and passaged by treatment with TrypLE Select Enzyme (Thermo Fisher Scientific) for 3 minutes at 37°C. After centrifugation, hiPSCs were seeded at a density of 5×10^4 cells/cm^2) onto iMatrix-511 coated surface and were subcultured every six days.

Hepatic differentiation

hiPSCs were seeded onto 35-mm dishes with a quartz bottom pretreated with Matrigel (BD science). The culture area was restricted by a silicone ring with an inner diameter of 15 mm. The 25-day stepwise differentiation was performed from the induction of DE cells, HB cells, and final hepatocyte-like cells.[25,26] For the differentiation info definitive endoderm cells, hiPSCs were cultured in RPMI1640 medium (Sigma-Aldrich) containing 100 ng/ml activin A (R&D Systems), 1×Gluta-MAX, and 1×B27 supplement minus vitamin A (Thermo Fisher Scientific) for 4 days. To induce the differentiation of hepatoblast-like cells, the medium was replaced to RPMI1640 medium which contained 20 ng/ml BMP4 (R&D Systems), 20 ng/ml FGF4 (R&D Systems), 1×GlutaMAX, and 1×B27 supplement minus vitamin A and cultured for 5 days. The hepatoblast-like cells were firstly cultured in RPMI1640 medium supplemented with 20 ng/ml HGF, 1×GlutaMAX, and 1×B27 Supplement Minus Vitamin A for 5 days and later cultured in Hepatocyte Culture Medium Bullet Kit™ (HCM, Lonza) with 20 ng/ml OsM for 11 days.

Live-cell Raman imaging

After washing by PBS and renewing with FluoroBrite DMEM (Thermo Fisher Scientific), living cells at different stages of hepatic differentiation were imaged by our homemade line-illumination Raman microscope.[43,44]. The excitation wavelength of 532 nm was generated by a CW laser (Millennia eV, Spectra-Physics) with a power density of 3 mW/μm^2 at the sample plane. To accelerate imaging speed, the laser light was shaped into a line using a cylindrical lens set to enable simultaneous detection of 400 spectra as one line. The incident light was focused on the sample using a water-immersion objective lens (CFI75 Apochromat 25×, NA 1.1; Nikon) mounted on an inverted microscope (ECLIPISE Ti2-E, Nikon). The Raman scattered light was collected by the same objective lens and then passed through a 532-nm long-pass edge filter (LP03-532RU-25, Semrock) to block the excitation light and Rayleigh scattered light. By placing a slit in front of the spectrometer, the line-illumination Raman microscopy achieved the axial resolution similar to the confocal effect.[45] Then the Raman scattered light passed into an imaging spectrometer (MK-300; Bunkoukeiki), dispersed by the grating (600 L/mm), and detected using a cooled CCD camera (PIXIS 400B; Teledyne Princeton Instruments) with an exposure time of 5 s per line. A single-axis galvanometer mirror was used to scan 126 lines per image, leading to a total of 50,400 (400 pixels × 126 lines) spectra for one image with an acquisition time less than 20 min. The pitch size of scanning was 1.6 μm.

Data processing

Raman hyperspectral images were processed as described previously.[43,44]. Briefly, cosmic rays were removed by a median filter, singular value decomposition (SVD) was applied to reduce noise, with loading vectors contributing to image contrast chosen. Following SVD processing,

the peak area of individual Raman peaks was utilized to map the intensity distribution of the designated Raman shifts.

Image-based quantitative analysis was conducted after reconstruction of hyperspectral Raman images. Merged Raman images at 940 cm^{-1} and 1000 cm^{-1} were utilized for the segmentation of cell bodies. For D25 HLCs we used a Raman image at 1636 cm^{-1} to avoid artefacts from the strong signal of lipid droplets. Following segmentation, the individual masks of cell bodies were applied to the Raman hyperspectral data to acquire averaged spectra per cell. The Raman data were preprocessed with cosmic ray removal but not with SVD processing to avoid the effect of the noise reduction in the quantitative analysis. The intensity of the target Raman shifts was calculated in terms of the peak area.

Immunofluorescence staining

The cell samples at different stages in hepatic differentiation were fixed in 4% paraformaldehyde (PFA) solution in PBS for 20 min at room temperature (RT). After permeabilizing with 0.1% Triton X-100 in PBS for 10 min, the cell samples were blocked with 4% bovine serum albumin for 1 h at RT. Then, the cell samples were incubated with a primary antibody in 1% bovine serum albumin overnight at 4°C, and next day with a secondary antibody solution in 1% bovine serum albumin for 1 h at RT. The primary antibodies and secondary antibodies used in this study were listed in Table S1 and S2. 1 μM DAPI solution (D1306; Invitrogen) was used to stain the cell nuclei for 20 min at RT. Fluorescent images were captured using a confocal laser scanning microscope (A1; Nikon).

PAS staining

The cultured cells were fixed in 4% PFA and incubated in 0.5% periodic acid solution (164-19705; Wako) for 5 min, rinsed in distilled water and incubated in Schiff's reagent (193-08445; Wako) for 15 min at RT. The cells were then washed with tap water for 2~3 times and slide-mounted for imaging.

Real-time RT-PCR analysis of gene expression

Total RNA was isolated from the cells using an RNA extraction kit (Isogen, Nippon Gene) following the manufacturer's instruction and DNA was removed by the treatment with DNase. 500 ng RNA was reverse transcribed using a Superscript VILO cDNA synthesis kit (11754050; Thermo Fisher Scientific). For real-time RT-PCR analysis, the mRNA expression was quantified SYBR Green PCR Master Mix (4309155; Thermo Fisher Scientific) on a StepOnePlus real-time PCR system (Thermo Fisher Scientific). The relative quantitation of target mRNA levels was performed by using the 2-ΔΔCT method. The level of each gene expression was normalized with that of glyceraldehyde 3-phosphate dehydrogenase (GAPDH). The PCR primer sequences were obtained from PrimerBank and are shown in Table S3.

Statistical analysis

The quantitative data presented in this study were obtained from three independent cultures. Statistical analysis was first assessed with one-way analysis of variance (ANOVA), and individual differences were tested using post hoc Tukey–Kramer's range tests according to unequal sample sizes. All calculations were performed using Origin 2019 (OriginLab Corporation, MA, USA). Statistical significance was set at $P < 0.05$: *** $P<0.001$; **$P<0.01$; *$P<0.05$; n.s. (not significant) $P \geq 0.05$.

ASSOCIATED CONTENT

AUTHOR INFORMATION

Corresponding Authors

Menglu Li – Department of Applied Physics, Osaka University, 2-1 Yamadaoka, Suita, Osaka 565-0871, Japan; AIST-Osaka University Advanced Photonics and Biosensing Open Innovation Laboratory, National Institute of Advanced Industrial Science and Technology (AIST), Suita, Osaka 565-0871, Japan; Email: menglu.li@ap.eng.osaka-u.ac.jp.

Katsumasa Fujita – Department of Applied Physics, Osaka University, 2-1 Yamadaoka, Suita, Osaka 565-0871, Japan; AIST-Osaka University Advanced Photonics and Biosensing Open Innovation Laboratory, National Institute of Advanced Industrial Science and Technology (AIST), Suita, Osaka 565-0871, Japan; Email: fujita@ap.eng.osaka-u.ac.jp.

Author contributions: M.Li, S.F. and K.F. conceived the concept; M.Li and Y.T. designed the experiments with the help of S.I., Y.Kanda, S.F., H.M. and K.F.; M.Li. and Y.T. performed the experiments; M.Li, Y.T., M.Lindley, G.K., S.I., Y.Kanda, Y.Kumamoto, S.F., H.M. and K.F. analyzed the data; Y.N. and S.F. provided tools for Raman measurement and analysis; Y.N., M.Li and G.K. carried out the optical alignment; M.Li and K.F. coordinated the project and supervised the research. M.Li, Y.T., M.Lindley and K.F. wrote the manuscript with input from all authors. All authors have read and agreed to submit the manuscript.

Competing interests: The authors declare no competing interests.

Supporting Information

The Supporting Information is available free of charge on the ACS Publication website.

The primary antibodies, the secondary antibodies, and the primers used in this research, gene expression levels of marker genes in plastic plates, time-course change of lipid-rich colony, screening hepatotoxicity in iCell hepatocytes and HepaRG cells using Raman imaging.

ACKNOWLEDGMENT

We thank Ms. K. Yamamoto and T. Yamashita for their excellent technical support. We thank Osaka University Photonics Center for providing support on common equipment. This research was supported by AIST-Osaka University Advanced Photonics and Biosensing Open Innovation Laboratory (PhotoBio-OIL), JST-CREST and JST COI-NEXT under Grant Numbers JPMJCR1925 and JPMJPF2009. M. Li. received Young Research Challenge funding under JST-CRES for this research.

Table of contents

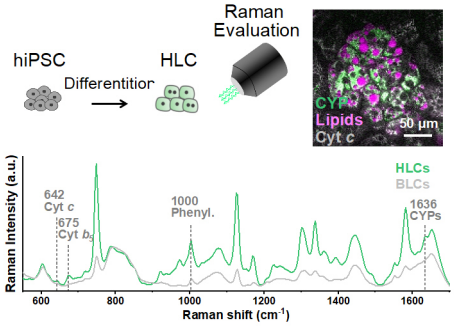

REFERENCES

1. Asrani, S. K.; Devarbhavi, H.; Eaton, J.; Kamath, P. S. Burden of liver diseases in the world. *J. Hepatol.* **2019**, *70*, 151-171.
2. Si-Tayeb, K.; Noto, F. K.; Nagaoka, M.; Li, J.; Battle, M. A.; Duris, C.; North, P. E.; Dalton, S.; Duncan, S. A. Highly efficient generation of human hepatocyte-like cells from induced pluripotent stem cells. *Hepatology* **2010**, *51*, 297-305.
3. Touboul, T.; Hannan, N. R.; Corbineau, S.; Martinez, A.; Martinet, C.; Branchereau, S.; Mainot, S.; Strick-Marchand, H.; Pedersen, R.; Di Santo, J.; Weber, A.; Vallier, L. Generation of functional hepatocytes from human embryonic stem cells under chemically defined conditions that recapitulate liver development. *Hepatology* **2010**, *51*, 1754-1765.
4. Hannan, N. R.; Segeritz, C. P.; Touboul, T.; Vallier, L. Production of hepatocyte-like cells from human pluripotent stem cells. *Nat. Protoc.* **2013**, *8*, 430-437.
5. Hannoun, Z.; Steichen, C.; Dianat, N.; Weber, A.; Dubart-Kupperschmitt, A. The potential of induced pluripotent stem cell derived hepatocytes. *J. Hepatol.* **2016**, *65*, 182-199.
6. Takayama, K.; Akita, N.; Mimura, N.; Akahira, R.; Taniguchi, Y.; Ikeda, M.; Sakurai, F.; Ohara, O.; Morio, T.; Sekiguchi, K.; Mizuguchi, H. Generation of safe and therapeutically effective human induced pluripotent stem cell-derived hepatocyte-like cells for regenerative medicine. *Hepatol. Commun.* **2017, *1*, 1058-1069.**
7. Takahashi, K.; Tanabe, K.; Ohnuki, M.; Narita, M.; Ichisaka, T.; Tomoda, K.; Yamanaka, S. Induction of pluripotent stem cells from adult human fibroblasts by defined factors. *Cell* **2007**, *131*, 861-872.
8. Aoi, T.; Yae, K.; Nakagawa, M.; Ichisaka, T.; Okita, K.; Takahashi, K.; Chiba, T.; Yamanaka, S. Generation of pluripotent stem cells from adult mouse liver and stomach cells. *Science* **2008**, *321*, 699-702.
9. Nagamoto, Y.; Takayama, K.; Ohashi, K.; Okamoto, R.; Sakurai, F.; Tachibana, M.; Kawabata, K.; Mizuguchi, H. Transplantation of a human iPSC-derived hepatocyte sheet increases survival in mice with acute liver failure. *J. Hepatol.* **2016**, *64*, 1068-1075.
10. Takebe, T.; Sekine, K.; Enomura, M.; Koike, H.; Kimura, M.; Ogaeri, T.; Zhang, R. R.; Ueno, Y.; Zheng, Y. W.; Koike, N.; Aoyama, S.; Adachi, Y.; Taniguchi, H. Vascularized and functional human liver from an iPSC-derived organ bud transplant. *Nature* **2013**, *499*, 481-484.
11. Clinical trial implementation for congenital urea cycle disorder using human ES cells. National Center for Child Health and Development, 2020. https://www.ncchd.go.jp/en/news/2020/pr_20200521-e.html (accessed December 2022).
12. Butler, H. J.; Ashton, L.; Bird, B.; Cinque, G.; Curtis, K.; Dorney, J.; Esmonde-White, K.; Fullwood, N. J.; Gardner, B.; Martin-Hirsch, P. L.; Walsh, M. J.; McAinsh, M. R.; Stone, N.; Martin, F. L. Using Raman spectroscopy to characterize biological materials. *Nat. Protoc.* **2016**, *11*, 664-687.
13. Ember, K. J. I.; Hoeve, M. A.; McAughtrie, S. L.; Bergholt, M. S.; Dwyer, B. J.; Stevens, M. M.; Faulds, K.; Forbes, S. J.; Campbell, C. J. Raman spectroscopy and regenerative medicine: a review. *NPJ Regen. Med.* **2017**, *2*, 12.
14. Albro, M. B.; Bergholt, M. S.; St-Pierre, J. P.; Vinals Guitart, A.; Zlotnick, H. M.; Evita, E. G.; Stevens, M. M. Raman spectroscopic imaging for quantification of depth-dependent and local heterogeneities in native and engineered cartilage. *NPJ Regen. Med.* **2018**, *3*, 3.

15. Hsu, C. C.; Xu, J.; Brinkhof, B.; Wang, H.; Cui, Z.; Huang, W. E.; Ye, H. A single-cell Raman-based platform to identify developmental stages of human pluripotent stem cell-derived neurons. *Proc. Natl. Acad. Sci. U. S. A.* **2020**, *117*, 18412-18423.
16. Brauchle, E.; Knopf, A.; Bauer, H.; Shen, N.; Linder, S.; Monaghan, M. G.; Ellwanger, K.; Layland, S. L.; Brucker, S. Y.; Nsair, A.; Schenke-Layland, K. Non-invasive chamber-specific identification of cardiomyocytes in differentiating pluripotent stem cells. *Stem Cell Rep.* **2016**, *6*, 188-199.
17. Wu, H. H.; Ho, J. H.; Lee, O. K. Detection of hepatic maturation by Raman spectroscopy in mesenchymal stromal cells undergoing hepatic differentiation. *Stem Cell Res. Ther.* **2016**, *7*, 6.
18. Tsikritsis, D.; Shi, H.; Wang, Y.; Velugotla, S.; Sršeň, V.; Elfick, A.; Downes, A. Label-free biomarkers of human embryonic stem cell differentiation to hepatocytes. *Cytometry A* **2016**, *89*, 575-584.
19. Pettinato, G.; Coughlan, M. F.; Zhang, X.; Chen, L.; Khan, U.; Glyavina, M.; Sheil, C. J.; Upputuri, P. K.; Zakharov, Y. N.; Vitkin, E.; D'Assoro, A. B.; Fisher, R. A.; Itzkan, I.; Zhang, L.; Qiu, L.; Perelman, L. T. Spectroscopic label-free microscopy of changes in live cell chromatin and biochemical composition in transplantable organoids. *Sci. Adv.* **2021**, *7*, eabj2800.
20. Hamada, K.; Fujita, K.; Smith, N. I.; Kobayashi, M.; Inouye, Y.; Kawata, S. Raman microscopy for dynamic molecular imaging of living cells. *J. Biomed. Opt.* **2008**, *13*, 044027.
21. Okada, M.; Smith, N. I.; Palonpon, A. F.; Endo, H.; Kawata, S.; Sodeoka, M.; Fujita, K. Label-free Raman observation of cytochrome *c* dynamics during apoptosis. *Proc. Natl. Acad. Sci. U. S. A.* **2012**, *109*, 28-32.
22. Hashimoto, A.; Yamaguchi, Y.; Chiu, L. D.; Morimoto, C.; Fujita, K.; Takedachi, M.; Kawata, S.; Murakami, S.; Tamiya, E. Time-lapse Raman imaging of osteoblast differentiation. *Sci. Rep.* **2015**, *5*, 12529.
23. Ichimura, T.; Chiu, L. D.; Fujita, K.; Kawata, S.; Watanabe, T. M.; Yanagida, T.; Fujita, H. Visualizing cell state transition using Raman spectroscopy. *PLoS One* **2014**, *9*, e84478.
24. Li, M.; Nawa, Y.; Ishida, S.; Kanda, Y.; Fujita, S.; Fujita, K. Label-free chemical imaging of cytochrome P450 activity by Raman microscopy. *Commun. Biol.* **2022**, *5*, 778.
25. Takayama, K.; Inamura, M.; Kawabata, K.; Katayama, K.; Higuchi, M.; Tashiro, K.; Nonaka, A.; Sakurai, F.; Hayakawa, T.; Furue, M. K.; Mizuguchi, H. Efficient generation of functional hepatocytes from human embryonic stem cells and induced pluripotent stem cells by HNF4α transduction. *Mol. Ther.* **2012**, *20*, 127-137.
26. Toba, Y.; Deguchi, S.; Mimura, N.; Sakamoto, A.; Harada, K.; Hirata, K.; Takayama, K.; Mizuguchi, H. Comparison of commercially available media for hepatic differentiation and hepatocyte maintenance. *PLoS One* **2020**, *15*, e0229654.
27. Wang, H.; Quiroga, A. D.; Lehner, R. Analysis of lipid droplets in hepatocytes. Analysis of lipid droplets in hepatocytes. *Methods Cell Biol.* **2013**, *116*, 107-127.
28. Naik, P. P.; Praharaj, P. P.; Bhol, C. S.; Panigrahi, D. P.; Mahapatra, K. K.; Patra, S.; Saha, S.; Bhutia, S. K. Mitochondrial heterogeneity in stem cells. *Adv. Exp. Med. Biol.* **2019**, *1123*, 179-194.
29. Kallepitis, C.; Bergholt, M. S.; Mazo, M. M.; Leonardo, V.; Skaalure, S. C.; Maynard, S. A.; Stevens, M. M. Quantitative volumetric Raman imaging of three dimensional cell cultures. *Nat. Commun.* **2017**, *8*, 14843.

30. Sirenko, O.; Hesley, J.; Rusyn, I.; Cromwell, E. F. High-content assays for hepatotoxicity using induced pluripotent stem cell-derived cells. *Assay Drug Dev. Technol.* **2014**, *12*, 43-54.
31. Czamara, K.; Majzner, K.; Pacia, M. Z.; Kochan, K.; Kaczor, A.; Baranska, M. Raman spectroscopy of lipids: a review. *J. Raman Spectrosc.* **46**, 4-20 (2015).
32. Lu, J.; Einhorn, S.; Venkatarangan, L.; Miller, M.; Mann, D. A.; Watkins, P. B.; LeCluyse, E. Morphological and functional characterization and assessment of iPSC-derived hepatocytes for in vitro toxicity testing. *Toxicol. Sci.* **2015**, *147*, 39-54.
33. Hinson, J. A.; Mays, J. B.; Cameron, A. M. Acetaminophen-induced hepatic glycogen depletion and hyperglycemia in mice. *Biochem. Pharmacol.* **1983**, *32*, 1979-1988.
34. Huang, R.; Okuno, H.; Takasu, M.; Takeda, S.; Kano, H.; Shiozaki, Y.; Inoue, K. Effects of rifampin on the glutathione depletion and cytochrome c reduction by acetaminophen reactive metabolites in an in vitro P450 enzyme system. *Jpn J. Pharmacol.* **2000**, *83*, 182-190.
35. Kinoshita, T.; Sekiguchi, T.; Xu, M. J.; Ito, Y.; Kamiya, A.; Tsuji, K.; Nakahata, T.; Miyajima, A. Hepatic differentiation induced by oncostatin M attenuates fetal liver hematopoiesis. *Proc. Natl. Acad. Sci. U. S. A.* **1999**, *96*, 7265-7270.
36. Zhang, W.; Li, W.; Liu, B.; Wang, P.; Li, W.; Zhang, H. E. Efficient generation of functional hepatocyte-like cells from human fetal hepatic progenitor cells in vitro. *J. Cell Physiol.* **2012**, *227*, 2051-2058.
37. Chen, R. J.; Zhang, G.; Garfield, S. H.; Shi, Y. J.; Chen, K. G.; Robey, P. G.; Leapman, R. D. Variations in Glycogen Synthesis in Human Pluripotent Stem Cells with Altered Pluripotent States. *PLoS One* **2015**, *10*, e0142554.
38. Hesseldahl, H.; Larsen, J. F. Ultrastructure of human yolk sac: endoderm, mesenchyme, tubules and mesothelium. *Am. J. Anat.* **1969**, *126*, 315-335.
39. D'Amour, K. A.; Agulnick, A. D.; Eliazer, S.; Kelly, O. G.; Kroon, E.; Baetge, E. E. Efficient differentiation of human embryonic stem cells to definitive endoderm. *Nat. Biotechnol.* **2005**, *23*, 1534-1541.
40. Fraga, A.; Ribeiro, L.; Lobato, M.; Santos, V.; Silva, J. R.; Gomes, H.; da Cunha Moraes, J. L.; de Souza Menezes, J.; de Oliveira, C. J.; Campos, E.; da Fonseca, R. N. Glycogen and glucose metabolism are essential for early embryonic development of the red flour beetle *Tribolium castaneum*. *PLoS One* **2013**, *8*, e65125.
41. Lee, W. M. Acetaminophen Toxicity: A History of Serendipity and Unintended Consequences. *Clin. Liver Dis. (Hoboken)* **2020**, *16*, 34-44.
42. Takayama, K.; Morisaki, Y.; Kuno, S.; Nagamoto, Y.; Harada, K.; Furukawa, N.; Ohtaka, M.; Nishimura, K.; Imagawa, K.; Sakurai, F.; Tachibana, M.; Sumazaki, R.; Noguchi, E.; Nakanishi, M.; Hirata, K.; Kawabata, K.; Mizuguchi, H. Prediction of interindividual differences in hepatic functions and drug sensitivity by using human iPS-derived hepatocytes. *Proc. Natl. Acad. Sci. U. S. A.* **2014**, *111*, 16772-16777.
43. Palonpon, A. F.; Ando, J.; Yamakoshi, H.; Dodo, K.; Sodeoka, M.; Kawata, S.; Fujita, K. Raman and SERS microscopy for molecular imaging of live cells. *Nat. Protoc.* **2013**, *8*, 677-692.
44. Li, M.; Liao, H. X.; Bando, K.; Nawa, Y.; Fujita, S.; Fujita, K. Label-free monitoring of drug-induced cytotoxicity and its molecular fingerprint by live-cell Raman and autofluorescence imaging. *Anal. Chem.* **2022**, *94*, 10019-10026.
45. Kawata, S.; Arimoto, R.; Nakamura, O. Three-dimensional optical-transferfunctionanalysis for a laser-scan fluorescence microscope with an extended detector. *J. Opt. Soc. Am.* **1991**, *8*, 171-175.